## This paper is published as part of a PCCP Themed Issue on:

# *Synergies between Experimental and Theoretical Studies of Gas Phase Reactions*

Guest Edited by: Paul Seakins (Leeds) and Struan Robertson (Accelrys, Cambridge and Leeds)

Published in issue 31, 2007 of PCCP

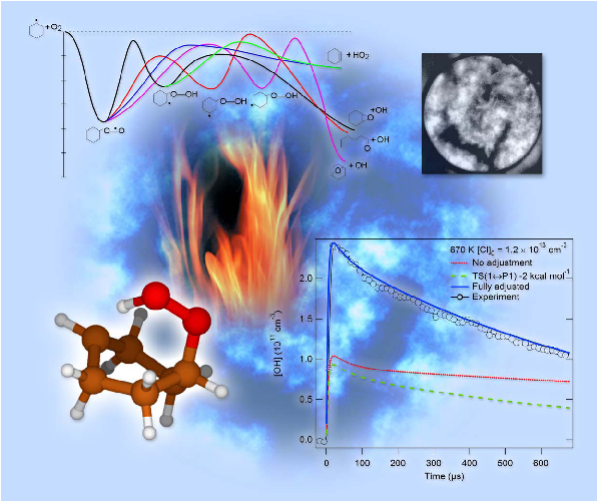


Image reproduced by permission of Dr Taatjes and Linda A.Houston for Sandia National Laboratories from *Phys.Chem.Chem.Phys.*, 2007, **9**, 4315-4331

Other papers published in this issue include:

**Direct detection of polyynes formation from the reaction of ethynyl radical ($C_2H$) with propyne ($CH_3$–C≡CH) and allene ($CH_2$=C=$CH_2$)**
Fabien Goulay, David L. Osborn, Craig A. Taatjes, Peng Zou, Giovanni Meloni and Stephen R. Leone, *Phys. Chem. Chem. Phys.*, 2007
**DOI:** 10.1039/b614502g

**Master equation methods for multiple well systems: application to the 1-,2-pentyl system**
Struan H. Robertson, Michael J. Pilling, Luminita C. Jitariu and Ian H. Hillier, *Phys. Chem. Chem. Phys.*, 2007
**DOI:** 10.1039/b704736c

***Ab initio* methods for reactive potential surfaces**
Lawrence B. Harding, Stephen J. Klippenstein and Ahren W. Jasper, *Phys. Chem. Chem. Phys.*, 2007
**DOI:** 10.1039/b705390h

**Visit the website for both cutting edge research papers and authoritative review articles by leaders in a range of fields**

**www.rsc.org/pccp**

# Determination of the rate constant and product channels for the radical–radical reaction NCO(X $^2\Pi$) + $C_2H_5$(X $^2A''$) at 293 K

**R. Glen Macdonald***

***Received 7th February 2007, Accepted 11th April 2007***
***First published as an Advance Article on the web 1st May 2007***
**DOI: 10.1039/b701900a**

The rate constant and product branching ratios for the reaction of the cyanato radical, NCO (X $^2\Pi$), with the ethyl radical, $C_2H_5$(X $^2A''$), have been measured over the pressure range of 0.28 to 0.59 kPa and at a temperature of 293 ± 2 K. The total rate constant, $k_1$, increased with pressure, $P$(kPa), described by $k_1 = (1.25 \pm 0.16) \times 10^{-10} + (4.22 \pm 0.35) \times 10^{-10}\ P$ cm$^3$ molecule$^{-1}$ s$^{-1}$. Three product channels were observed that were not pressure dependent: (1a) HNCO + $C_2H_4$, $k_{1a} = (1.1 \pm 0.16) \times 10^{-10}$, (1b) HONC + $C_2H_4$, $k_{1b} = (2.9 \pm 1.3) \times 10^{-11}$, (1c) HCN + $C_2H_4O$, $k_{1c} = (8.7 \pm 1.5) \times 10^{-13}$, with units cm$^3$ molecule$^{-1}$ s$^{-1}$ and uncertainties of one-standard deviation in the scatter of the data. The pressure dependence was attributed to a forth channel, (1d), forming recombination products $C_2H_5NCO$ and/or $C_2H_5OCN$, with pressure dependence: (1d) $k_{1d} = (0.090 \pm 1.3) \times 10^{-11} + (3.91 \pm 0.27) \times 10^{-10}\ P$ cm$^3$ molecule$^{-1}$ s$^{-1}$. The radicals were generated by the 248 nm photolysis of ClNCO in an excess of $C_2H_6$. Quantitative infrared time-resolved absorption spectrophotometry was used to follow the temporal dependence of the reactants and the appearance of the products. Five species were monitored, HCl, NCO, HCN, HNCO, and $C_2H_4$, providing a detailed picture of the chemistry occurring in the system. Other rate constants were also measured: ClNCO + $C_2H_5$, $k_{10} = (2.3 \pm 1.2) \times 10^{-13}$ , NCO + $C_2H_6$, $k_2 = (1.6 \pm 0.11) \times 10^{-14}$, NCO + $C_4H_{10}$, $k_4 = (5.3 \pm 0.51) \times 10^{-13}$, with units cm$^3$ molecule$^{-1}$ s$^{-1}$ and uncertainties of one-standard deviation in the scatter of the data.

## I. Introduction

The chemical interaction of two radicals is a class of reactions that plays an important role in combustion chemistry.[1] Radical–radical reactions can be either chain propagating or terminating events. In addition, they can lead to the generation of new species increasing the complexity of the chemical environment. The recombination of two radicals is directly connected to the reverse bond dissociation reaction through the equilibrium constant. In many cases, the study of the dissociation reaction is easier from the viewpoint of the recombination process because of the weaker temperature dependence of recombination rate constants.[2]

Radical–radical interactions have several unique features.[3] Firstly, the interaction of two species with unpaired electron spins always involves the participation of at least two potential energy surfaces (PESs) differing in spin multiplicity. If one of the radicals possesses electron angular momentum, multiple electronic manifolds for each spin manifold also result from the interaction. Secondly, the PES corresponding to a bonding interaction between the two radicals is attractive with no potential energy barrier along the reaction coordinate forming the recombination product. On this PES the system is chemically activated, and the energy in the newly forming bond can be redistributed leading to isomerization and/or bond breaking product channels. Radicals are reactive species, and direct bimolecular metathesis reactions can occur without complex formation. Thus, products can be formed by either a direct-abstraction or an addition-elimination pathway, and it is not generally easy to determine the dynamical route that produced a particular product channel.

Experimentally, the determination of a rate constant for a radical–radical reaction requires the measurement of the concentration of two transient species, and if product branching ratios are measured, the concentration of the products must be determined as well. For some reactions, these difficulties have been overcome, and real-time measurements of rate constants and product branching ratios have been made. For example, Knyazev and Slagle[4] studied a variety of alkyl radical–radical reactions, and in some cases, measured the product branching ratios.[5,6]

Theoretically, the calculation of a recombination rate constant requires a variational treatment,[7] and a description of the interaction between the two radicals in the region where chemical and long range forces are similar in magnitude. Recent calculations based on variable reaction coordinate transition state theory (VRC-TST) by Klipenstein *et al.*[8] have elucidated alkyl radical recombination reactions. However, the calculations do not address direct radical disproportionation or metathesis reactions that can also occur on PESs without energy barriers. Metathesis reactions occur at closer internuclear separations where chemical forces dominate. For

*Chemistry Division, Argonne National Laboratory, 9700 South Cass Avenue, Argonne, 60439-4831 Illinois, USA. E-mail: rgmacdonald@anl.gov; Fax: (630) 252-9292*

example, Harding *et al.*[9] calculated the total addition and abstraction rate constants as a function of temperature for the reactions, O + $C_2H_5$ and O + $C_2H_3$.

The cyanato radical (NCO, X $^2\Pi$) plays two important roles in combustion chemistry,[10] involving both $NO_X$ production and abatement. The NCO radical is involved in the generation of $NO_X$ by two mechanisms. These are the prompt production of $NO_X$, or the Fenimore mechanism[11] and the production of $NO_X$ from fuel fixed nitrogen sources. Both mechanisms are initiated by CN radical chemistry,[1] and the subsequent generation of NCO by the CN + $O_2$ reaction. Although there is considerable agreement between the predictions of various combustion mechanisms and experiment regarding $NO_X$ chemistry, there are still some areas of uncertainty.[12,13] Two $NO_X$ abatement strategies,[1] the $RaReNO_X$ and $NO_XOUT$ processes, involve NCO radical chemistry. These processes are based on the addition of cyanic acid ($(HONC)_3$) or urea ($(NH_2CO)$) to combustion exhaust gases, respectively, and the generation of HNCO leading to subsequent NCO chemistry removing $NO_X$.

The current work is a continuation of the study of the NCO radical with simple alkyl radicals.[14] The rate constant and product yields for the NCO and $C_2H_5$ reaction:

$$\mathbf{NCO} + C_2H_5 \rightarrow \mathbf{HNCO} + \mathbf{C_2H_4} \qquad \Delta H^0_{r,0} = -323.5 \pm 7\,\mathrm{kJ\,mol^{-1}} \tag{1a}$$

$$\rightarrow HOCN + \mathbf{C_2H_4}\ \Delta H^0_{r,0} = -221.0 \pm 8\,\mathrm{kJ\,mol^{-1}} \tag{1b}$$

$$\rightarrow \mathbf{HCN} + H_3CCHO\ \Delta H^0_{r,0} = -294 \pm 11\,\mathrm{kJ\,mol^{-1}} \tag{1c}$$

$$\rightarrow C_2H_5NCO/C_2H_5OCN \qquad \Delta H^0_{r,0} = -240/250 \pm 80\,\mathrm{kJ\,mol^{-1}} \tag{1d}$$

were measured at a temperature of 293 ± 2 K and pressure range of 2.1 to 4.5 Torr (1 Torr = 0.13332 kPa). The species in bold in the above reaction scheme were detected, along with HCl, using quantitative time-resolved infrared absorption spectroscopy. The rate constants for channels 1a, 1b and 1c were pressure independent while that for channel 1d was pressure dependent.

## II. Experimental

The apparatus and experimental procedure were the same as described recently, and only a brief overview is given here.[14–16] The reaction vessel was a vacuum-tight rectangular stainless-steel box about 110 × 110 × 7 cm that was continuously evacuated by a liquid-nitrogen-trapped mechanical pump. The gasses used in the experiment were supplied by AGA, and were used directly from their cylinders, with purities: Ar 99.9995%, $N_2O$ 99.98%, $C_2H_6$ 99.0%, $O_2$ 99.6%, and $n$-$C_4H_{10}$ 99.95%. The gases continuously flowed through the apparatus at a total flow rate between 300 and 500 sccm. Their partial pressures were determined from the total pressure and measured flow rates.

The method of generating and measuring the partial pressure of ClNCO has been described.[16] Briefly, ClNCO was generated by thermal decomposition of its trimer, and photolyzed at 248 nm using a Lamda Physik model 203 Compex excimer laser. At the entrance window to the reaction chamber, the photolysis laser fluence was varied between 5 and 20 mJ $cm^{-2}$ in a beam with dimensions 5 × 2 cm.

The infrared probe laser was a Burleigh model 20 single-mode color-center laser. The probe laser radiation was multi-passed through the photolysis region using White cell optics. The photolysis laser and probe laser were directly overlapped using a UV-IR dichroic mirror placed at Brewster's angle on the optical axis of the White cell. At the opposite end, the mirrors were protected from the UV laser radiation by a ZnS flat at Brewster's angle. The distance between these two optical elements provided a base optical path length of 139 ± 0.3 cm. Most of the data were collected with a total optical path length of 16.68 ± 0.04 m.

As will be discussed, the measurements on reaction 1 were done at low $C_2H_6$ pressures, ranging from 0.1 to 0.39 Torr. Higher $C_2H_6$ pressure experiments confirmed the measurements at low $C_2H_6$ pressures, and provided a measurement of the rate constant for the NCO + $C_2H_6$ reaction, $k_2$. The largest component in the gas mixture was generally $N_2O$. Separate experiments were also performed to measure the absorption cross section for a rotational transition in the HNCO fundamental $\nu_1$ vibrational band. These experiments were similar to those described in this section, and will be discussed in section III. D.

Time-resolved infrared absorption spectroscopy was used to monitor the temporal behavior of each detected species. Probe laser intensity fluctuations were the largest source of noise in the experiment. These were reduced by splitting the probe laser beam into equal intensity incident, $I_0$, and transmitted, $I$, beams. Each beam was detected by separate balanced InSb detectors. The difference signal, $I_0 - I$, was monitored by a wideband differential amplifier to suppress common-mode noise. A Con Optics Model Lass-II noise eater modulated the intensity of the $Kr^+$ ion laser that pumped the color-center laser in a feedback-control loop using a signal from the $I_0$ detector. Signal averaging, using a LeCroy Model 9410 digital oscilloscope further enhanced the signal-to-noise of the data.

Thermal lensing and refractive index changes in the optical elements exposed to the UV laser radiation induced background oscillations on the $I$ signal channel. These were removed by tuning to a nearby region of zero absorption and acquiring a background trace. The true differential absorption signal was determined by subtraction. Data collection was controlled by a laboratory computer.

## III. Results

### A. Concentration determination: NCO,[14] HCl,[17] $C_2H_4$,[18,19] and HNCO[20]

Each species was detected using isolated-rovibrational transitions originating from their ground vibrational levels. For a narrow-band source at frequency, $\nu$, the absorbance, $\ln(I_0(\nu)/I(\nu))$, is related to the concentration of species X, [X], by the Beer–Lambert law according to the product of path length, absorption coefficient, $\sigma(\nu)$, and concentration.[21] The $\sigma(\nu)$ is

 

given by the product of the line strength, $S_{ij}$, and the lineshape function, $g(\nu)$. At low pressures, pressure broadening can be neglected, and $g(\nu)$ is described by a normalized Doppler profile. Thus, at the peak of an absorption line, the absorption cross section, $\sigma_{pk}^{X}$, is related to the product of $S_{ij}$ and the inverse of the Doppler width. For the species detected in this work, it was estimated that pressure broadening would reduce $\sigma_{pk}^{X}$ by a few percent for pressures less than 5 Torr. The values for $\sigma_{pk}^{X}$ and the spectroscopic transitions are summarized in Table 1. Various spectral regions were scanned over for signatures of other species such as $C_2H_5$, $CH_3$, HNC, and NH, but none were detected either because of spectral congestion ($C_2H_5$ and $CH_3$) and/or the species were not produced in measurable concentrations ($>1 \times 10^{10}$ molecules $cm^{-3}$) (HNC and NH).

### B. Reaction model

The complete reaction mechanism[22–27] used to analyze the experimental data is given in Table 2. The enthalpies of formation[28–34] at 0 K, $\Delta H_{f,0}^{0}$, for the species in the model are listed in Table 3. The number of reactions that essentially accounted for all the chemistry in the system was smaller than the number in Table 2. The reactions in which the fractional integrated reaction contribution factors for a species were greater than 0.01 (the fractional $IRCF^{X}$ is the fraction of the total flux of X that passes through a reaction in which X is either a reactant or a product.) are given by:

$$ClNCO \xrightarrow{248\ nm} NCO + Cl$$

$$Cl + C_2H_6 \rightarrow HCl + C_2H_5 \quad (7)$$

$$NCO + C_2H_5 \rightarrow \text{products} \quad (1)$$

$$NCO + NCO \rightarrow N_2 + 2CO \quad (5)$$

$$NCO + C_2H_6 \rightarrow HNCO + C_2H_5 \quad (2)$$

$$C_2H_5 + C_2H_5 \rightarrow \text{products} \quad (9)$$

$$C_2H_5 + ClNCO \rightarrow NCO + C_2H_5Cl \quad (10)$$

$$X \xrightarrow{k_{diffusion}} \quad (11)$$

The reaction numbers refer to the numbering in Table 2.

Several comments are in order about the rate constants used in the data analysis. There have been several previous measurements[22,23,35] of $k_2$ near 295 K ranging from $2.1 \times 10^{-14}$ to $7.0 \times 10^{-14}$ $cm^3$ $molecule^{-1}$ $s^{-1}$. The data were analyzed using the slowest rate constant.[22] This value is in close agreement with the value of $k_2$ equal to $(1.6 \pm 0.11) \times 10^{-14}$ $cm^3$ $molecule^{-1}$ $s^{-1}$ determined in the present work. For reaction (9), both the rate constant and the branching between the

**Table 1** Spectroscopic transitions and $\sigma_{pk}^{X}$ for the species detected in this work

| Molecule | Upper level ← (0...) | Wavelength/μm | $\sigma_{pk}^{X}$/$cm^2$ $molecule^{-1}$ | Ref. |
|---|---|---|---|---|
| NCO | $(10^11)$ $P_{e/f}(12.5)$ | 3.165073 | $(3.13 \pm 0.12) \times 10^{-19}$ | 14 |
| HCl | $v = 1$ $R^{35}(3)$ | 3.354579 | $(7.57 \pm 0.08) \times 10^{-17}$ | 17 |
| | $v = 1$ $R^{35}(6)$ | 3.31737 | $(2.65 \pm 0.03) \times 10^{-17}$ | |
| $C_2H_4$ | $\nu_4$ $^rR_{70}(7)$ | 3.147379 | $(6.75 \pm 0.07) \times 10^{-19}$ | 18, 19 |
| | $\nu_4$ $^rR_{4,0}(4)$ | 3.177556 | $(1.38 \pm 0.014) \times 10^{-18}$ | |
| HNCO[a] | $\nu_1$ $^qR_0(16)$ | 2.816516 | $(5.2 \pm 0.57) \times 10^{-18}$ | This work |

[a] This HNCO band has been assigned in ref. 20.

**Table 2** Summary of the reactions and rate constants used to model the NCO + $C_2H_5$ system for 294 K

| No. | Reactants[a] | | Products | $k$/$cm^3$ $molecule^{-1}$ $s^{-1}$ [a] | Ref. |
|---|---|---|---|---|---|
| 1a | NCO + $C_2H_5$ | → | HNCO + $C_2H_4$ | Optimized | [b] |
| 1b | | → | HOCN + $C_2H_4$ | Optimized | [b] |
| 1c | | → | HCN + $C_2H_4O$ | Optimized | [b] |
| 1d | | → | $C_2H_5NCO/C_2H_5OCN$ | Optimized | [b] |
| 2 | NCO + $C_2H_6$ | → | HNCO + $C_2H_5$ | $(2.1 \pm 0.2) \times 10^{-14}$ | 22[c] |
| 3 | NCO + $C_2H_4$ | → | Products[d] | $(2.85 \pm 0.22) \times 10^{-12}$ | 23 |
| 4 | NCO + $n$-$C_4H_{10}$ | → | HNCO + $C_4H_9$[e] | $(6.1 \pm 0.3) \times 10^{-13}$ | 23 |
| 5 | NCO + NCO | → | $N_2$ + 2CO | $(5.0 \pm 2.0) \times 10^{-12}$ | 24 |
| 6 | NCO + Cl | → | NCl + CO | $(6.9 \pm 3.8) \times 10^{-11}$ | 16 |
| 7 | Cl + $C_2H_6$ | → | HCl + $C_2H_5$ | $(5.5 \pm 0.2) \times 10^{-11}$ | 25 |
| 8 | Cl + ClNCO | → | NCO + $Cl_2$ | $(2.4 \pm 1.6) \times 10^{-13}$ | 16 |
| 9a | $C_2H_5$ + $C_2H_5$ | → | $n$-$C_4H_{10}$ | $(2.4 \pm 0.42) \times 10^{-11}$ | 26 |
| 9b | | → | $C_2H_4$ + $C_2H_6$ | $(3.90 \pm 1.9) \times 10^{-12}$ | |
| 10 | $C_2H_5$ + ClNCO | → | NCO + $C_2H_5Cl$ | optimized | [b] |
| 11 | NCl + NCl | → | $Cl_2$ + $N_2$ | $(8.1 \pm 1.8) \times 10^{-12}$ | 27 |
| 12 | X | Diff. | X | measured/calculated | [f] |

[a] All reactions are second-order. [b] Measured in this work. [c] Measured in high $C_2H_6$ pressure experiments. [d] Likely products $H_2CCH(NCO)$ + H. [e] Measured in experiments used to determine $\sigma_{pk}^{HNCO}$. [f] See text.

**Table 3** Summary of the $\Delta H^0_{f,0}$ of the species in the NCO + $C_2H_5$ reaction model

| Species | $\Delta H^0_{f,0}$(X)/kJ mol$^{-1}$ | Ref. |
|---|---|---|
| NCO(X $^2\Pi$) | 128 ± 0.8 | 28 |
| Cl($^2$ P$_u$) | 119.62 ± 0.008 | 29 |
| $C_2H_5$(X $^2$A″) | 132 ± 4 | 30 |
| $C_2H_5$NCO | 20 ± 80$^a$ | This work |
| $C_2H_5$OCN | 10 ± 80$^a$ | This work |
| NCl(X$^3\Sigma^-$) | 325 ± 5 | 31 |
| $C_2H_6$ | −68.2 ± 0.3 | 30 |
| ClNCO | 53 ± 30 | 16 |
| HCl | −91.992 ± 0.006 | 29 |
| HNCO | −115.5 ± 0.8 | 28 |
| HOCN | −12.9 ± 1 | 28 |
| $C_2H_4$ | 61 ± 1 | 32 |
| CO | −113.8 ± 0.2 | 29 |
| HCN | 132 ± 4 | 32 |
| $H_3$CC(H)O | −166 ± 2$^b$ | 33 |
| $C_2H_3$NCO | 120$^c$ | |
| $C_4H_{10}$ | −97.5 ± 2 | 30 |
| $C_2H_5$Cl | −112.1 ± 1$^d$ | 34 |
| 1-$C_4H_9$ | 66.5$^d$ | 34 |
| 2-$C_4H_9$ | 70$^d$ | 34 |

$^a$ Estimated from theoretical calculations, see section III. F. $^b$ $\Delta H^0_{f,298}$ and corrected to 0 K. $^c$ Estimated from the C–N bond energy $C_2H_3NO_2$. $^d$ $\Delta H^0_{f,298}$.

recombination and disproportionation channels have been established.[5] Fortunately, $k_9$ is a factor of ten smaller than $k_1$ so that reaction (9) is a minor removal process for $C_2H_5$. The rate constant for reaction (7) is sufficiently large that the ethyl radicals are produced over a time-scale of a few tens of microseconds, and no other reactions contribute to the Cl atom loss. Hence, the initial concentrations of NCO and Cl are accurately determined by the initial HCl concentration.

When radicals are generated by photolysis, there is always the concern that excess energy will be deposited into vibrational motions of the products, and influence the subsequent kinetics. Using a recent estimate[16] of the bond dissociation energy of ClNCO to be 195 kJ mol$^{-1}$, there are 288 kJ mol$^{-1}$ of excess energy to be distributed between the relative translational motion of Cl and NCO and the internal energy in NCO. At a few Torr total pressure, translational and rotational energy are quickly thermalized, and only vibrational energy in NCO is of concern. The real extent of vibrational excitation in NCO is unknown but vibrational relaxation is rapid in NCO even in collisions with inert gases.[36] In the experiments reported here, $N_2O$ was the predominant carrier gas, and it is an efficient relaxation partner for vibrationally excited NCO.[37] Therefore, the vibrational energy levels of NCO are equilibrated to the temperature of the bath gas after a short induction period. There is no internal energy excitation in the $C_2H_5$ radical because reaction (7) is only slightly exothermic ($\Delta H^0_{f,0}$ = −11.2 kJ mol$^{-1}$).

The reaction time-scale is several milliseconds so that diffusion is an important removal process. The diffusional loss process is complicated by the geometry of the system, and two first-order rate constants differing in magnitude by about a factor of ten, describe the loss by diffusion.[14] Only the largest diffusional rate constant was considered in the data analysis of the first 5 ms of the concentration profiles. Binary diffusion constants were calculated for all species using the method developed by Fuller *et al.*,[38] and normalized to the observed diffusional loss rate constant for HCl. This procedure gave diffusional rate constants for the monitored stable species, HNCO, HCN and $C_2H_4$, within about 10% of their measured values, and provided good estimates for the unobserved species. The diffusional loss rate constants for NCO and $C_2H_5$ radicals were assumed to be the same as HNCO and $C_2H_4$, respectively.

### C. Determination of rate constants and product branching ratios

All rate constants were determined as described in recent works.[14,16] A single rate constant, in the reaction model of Table 2, noted by "optimized" in column 5, was varied until the sum of the squares of the residuals, $\chi^2_X$, between the experimental temporal concentration profiles of X and the model simulation was minimized. The fitting procedure also returned an estimate of the confidence limits in the value of the rate constant at the 68% level in the goodness-of-fit.

Reaction (10) is analogous to the $C_2H_5$ + $Cl_2$ reaction. Its inclusion in the reaction scheme improved the model fits to the NCO profile at long times. Three species were sensitive to the value of $k_{10}$, NCO, HNCO and $C_2H_4$, but only the NCO and $C_2H_4$ profiles were used in the data analysis for $k_{10}$ because their peak absorption coefficients (Table 1) were better determined. The procedure adopted to determine the optimum value of $k_{10}$ was similar to that described previously.[16] With $k_{1a}$ fixed by fitting the HNCO profile, a value of $k_{10}$ was chosen and each rate constant, $k_1$ and $k_{1b}$, was varied to define a minimum in $\chi^2_{NCO}(k_1, k_{10})$ and $\chi_{C_2H_4}{}^2(k_{1a+1b}, k_{10})$, respectively. The value of $k_{10}$ was incremented and the procedure repeated, until $\chi^2_{NCO}(k_1, k_{10})$ and $\chi_{C_2H_4}{}^2(k_{1a+1b}, k_{10})$ were defined as functions of $k_{10}$. The resulting parabolic curves were fit to a second-order polynomial to determine the values of $k_{10}$ that minimized $\chi^2_{NCO}(k_1, k_{10})$ and $\chi_{C_2H_4}{}^2(k_{1a+1b}, k_{10})$. Usually, the plot defining $\chi^2_{NCO}(k_1, k_{10})$ had the larger curvature and hence smaller uncertainty in the estimate of $k_{10}$. The optimum value of $k_{10}$ was taken as a weighted average of the two values, where the weights were the reciprocal of the 68% goodness-of-fit limits. The final values of $k_1$ and $k_{1a+1b}$ were determined by refitting the NCO and $C_2H_4$ profiles using this best estimate of $k_{10}$.

In an initial attempt to fit all the data, *i. e.* at low (<0.39 Torr) and high (>1.0 Torr) $C_2H_6$ pressures, the following strategy was adopted: $\sigma^{HNCO}_{pk}$ was treated as a variable because of its large uncertainty (Table 1), reaction $k_{1b}$ was not included in the reaction mechanism, and $k_2$ was fixed at the value in Table 2. No consistent values for $k_{1a}$ or $\sigma^{HNCO}_{pk}$ were found that described the complete data set, over this wide variation in $C_2H_6$ pressures (0.1 to 3.3 Torr). To deal with this, an alternate strategy was adopted: $\sigma^{HNCO}_{pk}$ was fixed at the value reported in Table 1, reaction (1b) was added to the mechanism, and $k_2$ was treated as a variable in analyzing the high $C_2H_6$ pressure experiments but fixed to the value in Table 2 in the analysis of low $C_2H_6$ pressure experiments. For the analysis of the low $C_2H_6$ pressure experiments, the HNCO temporal concentration profile was used to determine $k_{1a}$ by minimizing $\chi^2_{HNCO}$

 

with $k_1$ and $k_{10}$ fixed at the values determined by analyzing the NCO and $C_2H_4$ profiles, as discussed. With $k_{1a}$ known, $k_{1b}$ was found by minimizing $\chi_{C_2H_4}{}^2$ as a function of $k_{1b}$. In a similar fashion, $k_{1c}$ was determined by fixing the other rate constants and finding the minimum in $\chi^2_{HCN}$ as a function of $k_{1c}$. The rate constant for channel (1d), $k_{1d}$, was determined by subtracting the sum of the other three channel rate constants from $k_1$.

Typical experimental temporal concentration profiles are shown in Fig. 1 to 4. In each figure, panel (a) corresponds to the experimental profiles for NCO and HCl and panel (b) corresponds to the product profiles, $C_2H_4$, HNCO, and HCN. The open symbols are the experimental data shown every 10th point, the lines (dashed and solid) are the optimized fits to the appropriate species, and the dotted lines denote zero concentrations. The determination of $k_1$ and the product branching ratios were made under the conditions of low $C_2H_6$ pressures, as illustrated in Fig. 1 and 2. These experimental conditions

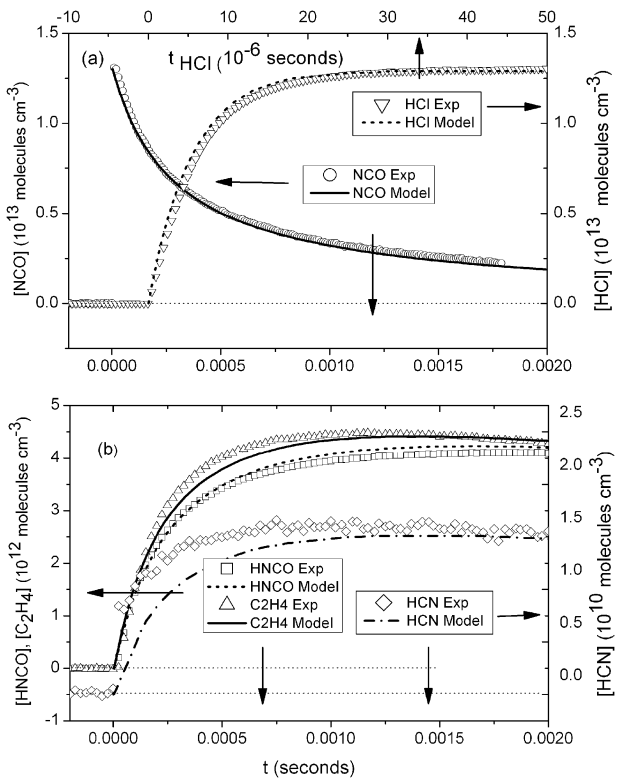


**Fig. 1** (a) Typical experimental temporal concentration profiles for NCO (○) and HCl (▽) observed at low total pressure and low $P_{C_2H_6}$. The data points are shown for every 10th point. The curves are the calculated model profiles for NCO (—) and HCl (···) using the optimum rate: $k_1 = (2.5 \pm 0.3) \times 10^{-10}$ cm$^3$ molecule$^{-1}$ s$^{-1}$ and $k_7 = (5.0 \pm 0.4) \times 10^{-11}$ cm$^3$ molecule$^{-1}$ s$^{-1}$, and $k_{10} = (2.9 \pm 1.0) \times 10^{-13}$ cm$^3$ molecules$^{-1}$ s$^{-1}$. (b) Same as (a) except for $C_2H_4$(△), HNCO(□), and HCN (◇). The curves are the model profiles for HNCO (···), $C_2H_4$ (—), and HCN (-•-) using the optimum rate constants: $k_{1a} = (1.2 \pm 0.12) \times 10^{-10}$, $k_{1b} = (1.7 \pm 0.5) \times 10^{-11}$, and $k_{1c} = (6.9 \pm 2.2) \times 10^{-13}$ cm$^3$ molecule$^{-1}$ s$^{-1}$. The conditions of the experiment were $P_{N_2O} = 1.82$, $P_{Ar} = 0.190$, $P_{C_2H_6} = 0.149$ and $P_{ClNCO} = 0.0078$ Torr at a temperature of 293 K.

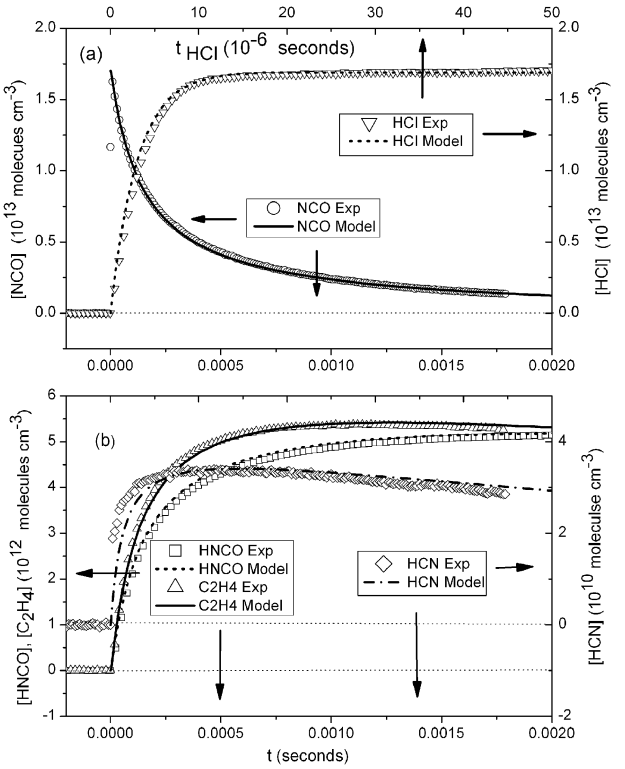


**Fig. 2** (a) Typical experimental temporal concentration profiles for NCO (○) and HCl (▽) observed at high total pressure and low $P_{C_2H_6}$. The data points are shown every 10th point. The curves are calculated model profiles for NCO (—) and HCl (···) using the optimum rate constants: $k_1 = (3.8 \pm 0.5) \times 10^{-10}$ cm$^3$ molecule$^{-1}$ s$^{-1}$ and $k_7 = (5.0 \pm 1.0) \times 10^{-11}$ cm$^3$ molecule$^{-1}$ s$^{-1}$, and $k_{10} = (1.0 \pm 1.0) \times 10^{-13}$ cm$^3$ molecules$^{-1}$ s$^{-1}$. (b) Same as (a) except for $C_2H_4$ (△), HNCO(□), and HCN (•). The curves are the model profiles for HNCO (···), $C_2H_4$ (—), and HCN (-···-): $k_{1a} = (1.3 \pm 0.3) \times 10^{-10}$, $k_{1b} = (3.1 \pm 0.3) \times 10^{-11}$, and $k_{1c} = (1.0 \pm 2.0) \times 10^{-13}$ cm$^3$ molecule$^{-1}$ s.$^{-1}$ The conditions of the experiment were $P_{N_2O} = 3.82$, $P_{Ar} = 0.384$, $P_{C_2H_6} = 0.172$ and $P_{ClNCO} = 0.013$ Torr at a temperature of 293 K.

and rate constant measurements are summarized in Table 4 and shown in Fig. 5.

A comparison between Fig. 1a and 2a shows that in the higher-pressure experiment NCO decays faster, although the initial NCO concentration is slightly larger. The rate constant analysis bears this observation out; $k_1$ is a factor 1.52 larger for a pressure change from 2.11 to 4.38 Torr. As can be seen from Table 4 and Fig. 5a, $k_1$ and $k_{1d}$ were pressure dependent but the other rate constants were independent of pressure (Fig. 5b and c).

In Fig. 1a and 2a, the model calculated HCl profiles were generated by determining optimum values for $k_7$ instead of the value listed in Table 2. Under high $P_{C_2H_6}$ conditions, Fig. 2a and 4a, the appearance rate of HCl was too large to provide an estimate for $k_7$. The analysis for $k_7$ yielded a value of $(4.7 \pm 0.26) \times 10^{-11}$ cm$^3$ molecule$^{-1}$ s$^{-1}$, where the uncertainty is one-standard deviation from the average, which is about 15% less than the more precise measurements of Pilgrim *et al.*[25] No attempt was made to provide an improved measurement for $k_7$. The $C_2H_6$ flow meter was used to cover the complete flow range of $C_2H_6$ (up to 400 sccm) and for low $C_2H_6$ pressures

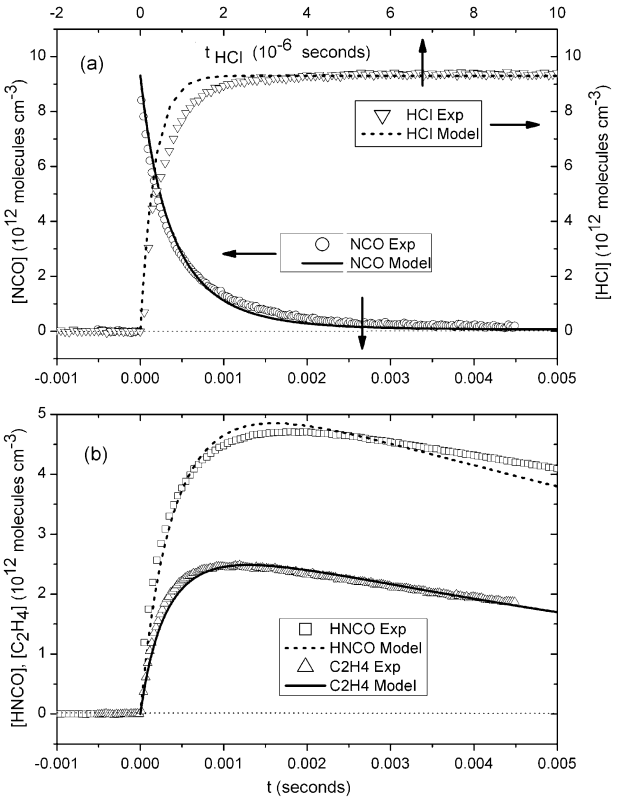


**Fig. 3** (a) Typical experimental temporal concentration profiles for NCO (○) and HCl (▽) observed at low total pressure and high $P_{C_2H_6}$. The data points are shown every 10th point. The curves are calculated model profiles for NCO (—) and HCl (···). For $k_2 = 1.6 \times 10^{-14}$ cm$^3$ molecules$^{-1}$ s$^{-1}$, the optimum value for $k_1$ was $(2.2 \pm 0.6) \times 10^{-10}$ cm$^3$ molecules$^{-1}$ s$^{-1}$. (b) Same as (a) except for $C_2H_4$ (△) and HNCO (□). The curves are the model profiles for HNCO (···) and $C_2H_4$ (—) using the optimum rate constants: $k_{1a} = (9.3 \pm 0.11) \times 10^{-11}$, $k_{1b} = (1.9 \pm 0.3) \times 10^{-11}$ cm$^3$ molecule$^{-1}$ s$^{-1}$. The conditions of the experiment were $P_{C_2H_6} = 1.55$, $P_{Ar} = 0.166$, and $P_{ClNCO} = 0.005$ Torr, at a temperature of 293 K.

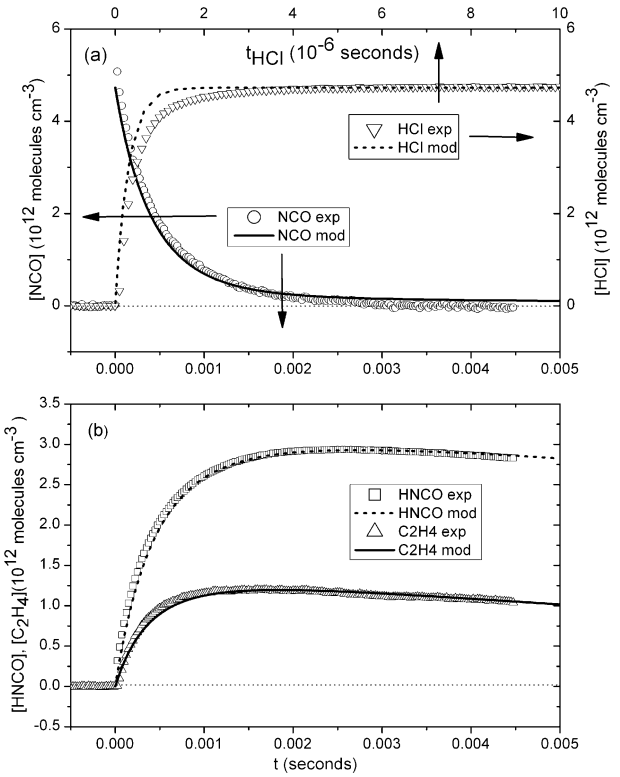


**Fig. 4** (a) Typical experimental temporal concentration profiles for NCO (○) and HCl (▽) observed at high total pressure and high $P_{C_2H_6}$. The data points are shown every 10th point. The curves are the model profiles for NCO (—) and HCl (···). For $k_2 = 1.6 \times 10^{-14}$ cm$^3$ molecules$^{-1}$ s$^{-1}$, the optimum value for $k_1$ was $(3.3 \pm 0.7) \times 10^{-10}$ cm$^3$ molecules$^{-1}$ s$^{-1}$. (b) Same as (a) except for $C_2H_4$ (△) and HNCO (□). The curves are the model profiles for HNCO (···) and $C_2H_4$ (—) using the optimum rate constants for each channel: $k_{1a} = (1.2 \pm 0.11) \times 10^{-10}$, $k_{1b} = (3.9 \pm 0.5) \times 10^{-11}$ cm$^3$ molecule$^{-1}$ s.$^{-1}$ The conditions of the experiment were $P_{C_2H_6} = 1.78$, $P_{N_2O} = 1.75$, $P_{Ar} = 0.38$, and $P_{ClNCO} = 0.01$ Torr, at a temperature of 294 K.

small $C_2H_6$ flows resulted in a larger uncertainty in the $C_2H_6$ partial pressure. None of the rate constant determinations for reaction (1) depended on the accuracy of the $C_2H_6$ pressure measurement.

It can be seen from Fig. 1b and 2b that the concentration of $C_2H_4$ is slightly larger than the concentration of HNCO, indicating another source of $C_2H_4$ besides reaction (1a). This other source was attributed to reaction (1b). When $k_{1b}$ was included in the reaction scheme, the calculated temporal concentration profiles for HNCO and $C_2H_4$ were in good agreement with the experimental profiles over the complete observation time-scale. This was also the case under high $C_2H_6$ pressure conditions, as seen in Fig. 3b and 4b. Note too, there is a difference in the shape of the $C_2H_4$ and HNCO profiles due to their slightly different chemistry. The model calculations reproduce this difference quite well.

The only product observed for channel (1c) was HCN with the $C_2H_4O$ coproduct assumed to be $CH_3CHO$, the most exothermic channel. This channel accounted for less than 0.4% of the product yield for reaction (1), and only a few measurements were made on its yield. As can be seen in Fig. 1b and 2b, the rise in the experimental HCN profile is faster than the model predictions. Similar behavior was observed for the HCN/HNC product channels in the NCO + $CH_3$ reaction.[14] In this case, this was attributed to rapid vibrational relaxation of excited HCN/HNC bending modes populating the ground vibrational level. Likely, the situation is similar for reaction (1). Note the better agreement for the appearance of HCN at higher $N_2O$ pressure, Fig. 2b compared to Fig. 1b, supports this speculation.

There is considerable excess energy released in reaction (1), and it is likely that some of this energy was deposited as vibrational energy in the products. Indeed, in the similar Cl + $C_2H_5$ → HCl + $C_2H_4$ reaction, the vibrational energy distribution in the HCl product has been measured[39] and vibrationally excited $C_2H_4$ has been observed.[40] An initial population inversion, indicated by negative absorption signals, was observed near time equal to zero on the HNCO profiles, but its duration was only a few microseconds. If vibrational relaxation were slow, the concentration and rate of appearance of the probed species would be underestimated. For a polyatomic molecule, the slowest vibrational relaxation step is

 

**Table 4** Summary of the experimental conditions and rate constant determinations for conditions with low $C_2H_6$ pressures

| Partial pressure/Torr | | | | [NCO][a] | | Rate constants/cm$^3$ molecule$^{-1}$ s$^{-1}$ | | | |
|---|---|---|---|---|---|---|---|---|---|
| $P_{N_2O}$ | $P_{Ar}$ | $P_{C_2H_6}$ | $P_{ClNCO}$ | $10^{13}$ | $k_1$ ($10^{-10}$) | $k_{1a}$ ($10^{-10}$) | $k_{1b}$ ($10^{-11}$) | $k_{1c}$ ($10^{-13}$) | $k_{10}$ ($10^{-13}$) |
| 1.76 | 0.187 | 0.148 | 0.0059 | 0.630 | 2.8(.13)[b] | 1.21(.02) | 3.4(.5) | | 2.0 (1.0) |
| 1.76 | 0.188 | 0.148 | 0.0076 | 0.667 | 2.6(.3) | 1.03(.03) | 3. 6(.5) | | 5.8(4.0) |
| 1.77 | 0.189 | 0.150 | 0.0089 | 1.06 | 2.8(.2) | 1.15(.05) | 2.5(.6) | | 1.0 (1.0) |
| 1.78 | 0.189 | 0.150 | 0.0078 | 1.25 | 3.0(.35) | 1.27(.07) | 2.2(.6) | | 0.5( 2.0) |
| 1.83 | 0.188 | 0.0964 | 0.010 | 0.907 | 2.0(.5) | 0.87(.17) | 3.7(.8) | | 3.7( 3.7) |
| 1.83 | 0.188 | 0.0964 | 0.010 | 0.907 | 2.4(.3) | 0.95(.15) | 3.4(.7) | | 2.2 (2.0) |
| 1.83 | 0.189 | 0.0943 | 0.011 | 0.883 | 2.4 (.2) | 1.1(.2) | 2.8(.65) | 7.3(2.3) | 1.5(1.0) |
| 1.83 | 0.190 | 0.0950 | 0.0075 | 1.35 | 1.8(.23) | 0.87(.4) | 1.7(.5) | | 4.9 (3.0) |
| 1.83 | 0.190 | 0.0950 | 0.0075 | 1.30 | 2.5(.3) | 1.16(.12) | 1.7(.5) | 6.9(2.0) | 2.9(2.9) |
| 3.23 | 0.401 | 0.318 | 0.014 | 1.03 | 3.1(.15) | 1.0(.05) | 3.0(.35) | | 0.5(1.5) |
| 3.23 | 0.401 | 0.318 | 0.014 | 1.00 | 3.0(.2) | 0.98(.08) | 3.0(.3) | | 2.0(1.5) |
| 3.83 | 0.386 | 0.173 | 0.013 | 1.77 | 3.5(.4) | 1.13(.3) | 2.9(.3) | | 1.0 (1.0) |
| 3.83 | 0.386 | 0.173 | 0.013 | 1.70 | 3.8(.48) | 1.28 (.3) | 3.1(.30) | 10. (2.0) | 1.0 (1.0) |
| 3.83 | 0.386 | 0.173 | 0.013 | 0.909 | 3.8(.35) | 1.19(.05) | 1.3(.25) | | 3.4(1.3) |
| 3.83 | 0.386 | 0.173 | 0.013 | 0.849 | 4.0(.6) | 1.42( .06) | 0.58(.2) | | 1.0(1.0) |
| 3.86 | 0.389 | 0.175 | 0.0089 | 0.860 | 4.2(.7) | 1.43(.06) | 2.4(.75) | | 1.5(1.5) |
| 3.86 | 0.389 | 0.175 | 0.0089 | 0.866 | 3.4(.25) | 1.20( .04) | 3.0(.7) | | 6.0(2.5) |
| 3.86 | 0.389 | 0.175 | 0.0089 | 0.844 | 3.8(.30) | 1.31(.02) | 2.7(.65) | 9.8(1.8) | 4.6 (3.0) |
| Average | | | | | [c] | 1.14 | 2.9 | 8.7 | 2.3 |
| Standard deviation | | | | | | 0.17 | 1.3 | 1.5 | 1.2 |

[a] Units molecules cm$^{-3}$. [b] Numbers in parentheses are the uncertainties at the 68% level of confidence in the goodness-of-fit. [c] Pressure dependent.

the relaxation of the lowest energetic level, a *V–R,T* process; higher vibrational levels rapidly equilibrate by *V–V* processes.[41] In the present experiments, the bath gas was either $N_2O$, $C_2H_6$ or both, and both molecules have vibrational energy levels lower in energy or nearly so than the lowest vibrational energy level in HNCO, $\nu_5$ = 574 cm$^{-1}$, and $C_2H_4$, $\nu_{10}$ = 826 cm$^{-1}$. Thus, vibrational relaxation is expected to be facile for each molecule in collisions with $N_2O$ or $C_2H_6$. The HNCO molecule is a transient species, and no information on the vibrational relaxation of HNCO was found. However, except for the high frequency $\nu_1$ mode in HNCO, its vibrational frequencies are similar to NCO, and the vibrational relaxation of HNCO should be similar to NCO.[36,37] Vibrational relaxation in $C_2H_4$ has been investigated,[42,43] and the *V–T, R* relaxation of the lowest excited vibrational level was found to be rate limiting. Yaun and Flynn have measured the *V–T, R* rate constant of $C_2H_4$ with $C_2H_6$ to be $2.8 \times 10^{-12}$ cm$^3$ molecule$^{-1}$ s$^{-1}$. As is evidenced in Fig. 1b to 4b, there was no difference in the appearance rate of $C_2H_4$ or HNCO as a function of total pressure or $C_2H_6$ partial pressure, so that vibrational energy redistribution in $C_2H_4$ and HNCO was rapid on the time-scale of the reactions producing them.

Comparing the NCO profiles for low (Fig. 1a and 2a) and high (Fig. 3a and 4a) $C_2H_6$ pressure experiments, immediately reveals the influence of reaction (2). At high $C_2H_6$ pressure (Fig. 3a and 4a), the NCO profiles are more exponential in appearance. As already noted, there is considerable uncertainty in the reported[22,23,35] values for $k_2$; thus, the consistency of the measurements made under low $C_2H_6$ pressures was examined by analyzing the high $C_2H_6$ pressure experiments to determine $k_2$ independently. Under these conditions, the procedure used to determine $k_1$ and $k_2$ was similar to that described in the determination of $k_{10}$. However, both $\chi^2_{NCO}(k_1, k_2)$ and $\chi^2_{HNCO}(k_1, k_2)$ curves had very small curvatures; hence, the range of acceptable values of $k_1$ and $k_2$ was broad. Generally, a value of $k_1$ was found that agreed with $k_1$ determined under low $C_2H_6$ pressures, and the final $k_2$ value determined. The experimental conditions and results of this analysis are summarized in Table 5.

A notable feature of the results summarized in Table 4 and illustrated in Fig. 5a is the pressure dependence of $k_1$. Over this pressure range $k_1$ is described by $(1.25 \pm 0.16) \times 10^{-10} + (5.63 \pm 0.47) \times 10^{-11}$ *P*(Torr) cm$^3$ molecules$^{-1}$ s$^{-1}$. The pressure dependence is due to the recombination channel and $k_{1d}$ is given by $(0.090 \pm 1.3) \times 10^{-11} + (5.21 \pm 0.36) \times 10^{-10}$ *P*(Torr) cm$^3$ molecules$^{-1}$ s$^{-1}$. As is evident from Table 4 and shown in Fig. 5b, $k_{1a}$ and $k_{1b}$ were pressure independent, and have the values $(1.14 \pm 0.17) \times 10^{-10}$ and $(2.9 \pm 1.3) \times 10^{-11}$ cm$^3$ molecule$^{-1}$ s$^{-1}$, respectively, where the uncertainty is one-standard deviation from the average, $1\sigma$. Fig. 5c shows the measurements for $k_{1c}$, and within the scatter of the data, $k_{1c}$ appears to be pressure independent with a value of $(8.7 \pm 1.5) \times 10^{-13}$ cm$^3$ molecule$^{-1}$ s$^{-1}$. The last column of Table 4 lists the measurements of $k_{10}$ to be $(2.3 \pm 1.2) \times 10^{-13}$ cm$^3$ molecule$^{-1}$ s$^{-1}$ with uncertainty of $1\sigma$.

At high $C_2H_6$ pressures, independent measurements were made of $k_1$, $k_{1a}$, and $k_{1b}$ (Table 5) that were in good agreement with those made at low $C_2H_6$ pressures (Table 4). However, there was a high degree of correlation between $k_1$ and $k_2$, and the high $C_2H_6$ pressure measurements were not considered as reliable as the low pressure ones. The value found for $k_2$ is summarized in the last column in Table 5 and is $(1.6 \pm 0.11) \times 10^{-14}$ cm$^3$ molecule$^{-1}$ s$^{-1}$, where the uncertainty is $1\sigma$.

### D. Determination of $\sigma_{pk}^{HNCO}$

In order to determine the product branching into channel (1a), it is necessary to measure the absorption coefficient for a suitable spectroscopic transition in HNCO. However, the generation of pure samples of HNCO is not straightforward.[24] Thus, HNCO was generated *in situ* from the reaction of NCO + *n*-$C_4H_{10}$ using ClNCO as the NCO precursor. The initial

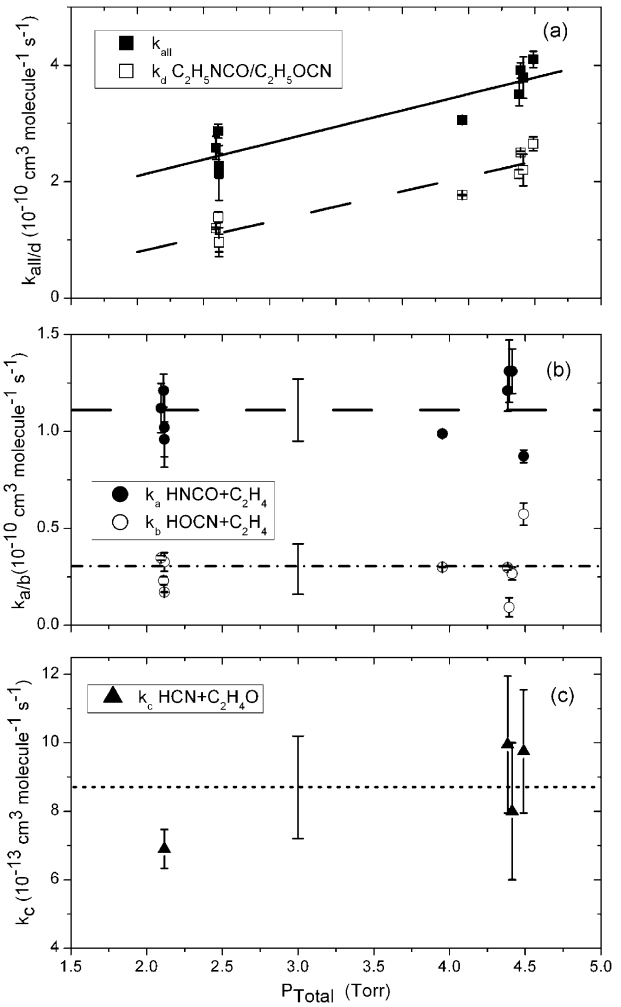


**Fig. 5** (a) Summary of the determination of the $k_1$ (■) and $k_{1d}$ (□) as a function of the total pressure. Only the low $P_{C_2H_6}$ data, Table 4, were used to determine the rate constants associated with reaction (1). The error bars are the uncertainty in the optimized values of $k_1$ at the 68% confidence level. The pressure dependence was allocated to the recombination channel. The lines are a linear fit to the data points. (b) Similar to (a) except a summary of the determination of the optimum values for $k_{1a}$ (●) and $k_{1b}$ (○). The dashed lines are the average values listed in Table 4 and the error bar attached to the lines the standard deviation. (c) Similar to (a) and (b) except for the determination of $k_{1c}$ (▲). Although there is an apparent pressure dependence on $k_{1c}$, the scatter is too large to be conclusive.

radical concentration was again determined from the HCl concentration generated in the Cl + $n$-$C_4H_{10}$ reaction. The rate constant for the NCO + $n$-$C_4H_{10}$ reaction is sufficiently large[23] that all the NCO radicals can be scavenged in a few hundred microseconds at modest pressures of $n$-$C_4H_{10}$, minimizing secondary loss processes. The complete reaction mechanism[44–47] used in the data analysis is given in Table 6.

The products of reaction (4) have not been conclusively established but a recent study[23] of the yield of HNCO from the reaction of NCO with a variety of alkanes and alkenes provides strong evidence that HNCO is the dominant channel. Both reactions (4) and (16) produce 1-$C_4H_9$ and 2-$C_4H_9$ radicals (Table 6) so that the reaction of NCO with these radicals was suppressed by the addition of excess $O_2$, as done by Maricq *et al.*[40] At the $O_2$ pressures used in the experiment, the rate of reaction (18) was sufficiently rapid that reactions (12), (13) and (14) made no significant contributions to the removal of NCO. Reaction (15) is a potential loss process for NCO that might not generate HNCO. The butylperoxide radical could decompose to the corresponding alkene + $HO_2$ products; however, no information was found on this pathway and it was not included in the mechanism.

The determinations of $k_4$ and $\sigma_{pk}^{HNCO}$ were made in an iterative manner. The first estimate of $k_4$ was made using the NCO profile. A value for $\sigma_{pk}^{HNCO}$ was then found by varying $\sigma_{pk}^{HNCO}$ to minimize $\chi^2_{HNCO}$ for the model and experimental HNCO profiles generated using the estimate of $k_4$ given from the NCO profile analysis. The value of $k_4$ was then revised by fitting the new HNCO experimental profile generated with the estimate of $\sigma_{pk}^{HNCO}$. Further iterations in $\sigma_{pk}^{HNCO}$ and $k_4$ resulted in changes of less than 2%. Values of $k_4$ determined by fitting the NCO profile were usually about 10% larger than those determined fitting the HNCO profile. This was attributed to the loss of NCO by reaction (4) before vibrational equilibration of NCO was complete. Under conditions of vibrational disequilibrium, monitoring only the ground state of NCO is not a true measure of the total NCO concentration. Evidence for this comes from the systematic under prediction of the initial NCO concentration determined by extrapolating the NCO profile back to time zero compared to the initial NCO concentration determined from the HCl profile.

Typical experimental profiles for HCl, HNCO, NCO, and their model simulations are shown in Fig. 6, and the experimental conditions and results are summarized in Table 7. Fig. 6a shows the initial 10 μs of the HCl profile and 450 μs of the HNCO profile. The model calculations presented in the figure reflect the last iteration to determine $k_4$ and $\sigma_{pk}^{HNCO}$ using the HNCO profile. For this calculation, $k_{15}$ was set to $1.0 \times 10^{-12}$ cm$^3$ molecule$^{-1}$ s$^{-1}$. With this value of $k_{15}$, the fraction on NCO removed by reaction 15 was $7 \times 10^{-4}$ but increased to 0.033 for $k_{15}$ equal to $5.0 \times 10^{-11}$ cm$^3$ molecule$^{-1}$ s$^{-1}$. Similar behavior was found in the simulations of the other experimental runs. It is unlikely that $k_{15}$ would be substantially larger than $k_4$ and it, therefore, had a small effect on the measurement of $\sigma_{pk}^{HNCO}$.

From Table 7, the value of $k_4$ determined fitting the NCO profile was $(5.7 \pm 0.86) \times 10^{-13}$ cm$^3$ molecules$^{-1}$ s$^{-1}$ and that determined fitting the HNCO profile was $(5.3 \pm 0.51) \times 10^{-13}$ cm$^3$ molecules$^{-1}$ s$^{-1}$, where the uncertainty is $1\sigma$. The value from the HNCO profile analysis was taken as the more reliable measurement. There is only one previous measurement of $k_4$. Park and Hershberger[23] found $k_4$ equal to $(6.1 \pm 0.3) \times 10^{-13}$ cm$^3$ molecules$^{-1}$ s$^{-1}$ at 296 K, and within the scatter of the measurements, the agreement is good.

### E. Reaction contribution factor analysis

It is important to have some measure of the influence an individual reaction has on the chemistry in a chemical reaction mechanism. One useful measure is a reaction contribution factor analysis[48] particularly when both concentrations and rate constants are important. An IRCF analysis was done for

 

**Table 5** Summary of the experimental conditions and rate constant[a] determinations for conditions of high $C_2H_6$ pressure

| Partial pressure/Torr | | | | [NCO] | Rate constants/cm$^3$ molecule$^{-1}$s$^{-1}$ [c] | | | | |
|---|---|---|---|---|---|---|---|---|---|
| $P_{C_2H_6}$ | $P_{N_2O}$ | $P_{Ar}$ | $P_{ClNCO}$ | ($10^{12}$)[b] | $k_1$ ($10^{-10}$) | $k_{1a}$ ($10^{-10}$) | $k_{1b}$ ($10^{-11}$) | $k_{1d}$ ($10^{-10}$) | $k_2$ ($10^{-14}$) |
| 1.55 | 0.0 | 0.161 | 005 | 8.51 | 2.5 ± 0.40 | 0.91 ± 0.10 | 2.8 ± 0.40 | 1.3 | 1.6 |
| 1.55 | 0.0 | 0.161 | 0.005 | 4.80 | 2.2 ± 0.30 | 1.1 ± 0.1 | 1.0 ± 0.30 | 1.1 | 1.7 |
| 3.25 | 0.0 | 0.338 | 0.005 | 8.40 | 2.7 ± 0.80 | 0.92 ± 0.5 | 0.0 | 1.8 | 1.6 |
| 1.55 | 0.0 | 0.166 | 0.005 | 9.20 | 1.7 ± 0.3 | 1.08 ± 0.11 | 2.2 ± 0.6 | 0.43 | 1.4 |
| 1.55 | 0.0 | 0.166 | 0.005 | 9.31 | 2.2 ± 0.50 | 0.91 ± 0.09 | 1.9 ± 0.30 | 1.1 | 1.6 |
| 3.15 | 0.0 | 0.349 | 0.010 | 20.3 | 3.1 ± 0.5 | 1.0 ± 0.15 | 2.0 ± 0.4 | 1.9 | 1.4 |
| 1.03 | 2.44 | 0.394 | 0.006 | 5.42 | 2.3 ± 0.4 | 1.2 ± 0.08 | 0.7 ± 0.6 | 1.1 | 1.4 |
| 1.55 | 1.94 | 0.387 | 0.006 | 5.27 | 2.2 ± 0.4 | 1.1 ± 0.1 | 1.7 ± 0.8 | 0.988 | 1.4 |
| 1.75 | 1.78 | 0.383 | 0.01 | 4.73 | 3.3 ± 0.7 | 1.2 ± 0.1 | 3.9 ± 0.4 | 1.8 | 1.6 |
| Average | | | | | [d] | 1.0 | 1.7 | [d] | 1.6 |
| Standard deviation | | | | | | 0.11 | 0.14 | | 0.11 |

[a] $k_{10}$ was fixed at $2.3 \times 10^{-13}$ cm$^3$ molecule$^{-1}$ s$^{-1}$. [b] Units molecule cm$^{-3}$. [c] The uncertainties are the 68% level of confidence in the goodness-of-fit. [d] Pressure dependent.

every model simulation. An example of an IRCF analysis for the experiment illustrated in Fig. 1 is shown in Fig. 7. The IRCF$^X$s are expressed as a fraction of the total amount of species × produced or removed in the system. As indicated by the IRCF$^{NCO}$ and IRCF$^{C_2H_5}$ plots in Fig. 7a and b, reaction (1) accounted for nearly 80% of the total removal of both NCO and $C_2H_5$, and only small fractions were removed by diffusion and reaction (9). Under low $C_2H_6$ pressure conditions, reaction (2) accounted for about 10% of the total removal of NCO and production of $C_2H_5$, as indicated in Fig. 7. The general behavior of the ICRF$^X$s, as outlined in Fig. 7 was observed in all the experiments.

### F. Theoretical estimates of the bond dissociation energies of $C_2H_5$–NCO and $C_2H_5$–OCN

The recombination channel accounts for over half of the products in reaction (1), but neither possible recombination product was detected in the present experiments. A theoretical estimate of the rate constant for this channel would be an important clue as to the dynamics of reaction (1). Furthermore, no experimental measurements or theoretical estimates could be found for the heat of formation for either $C_2H_5NCO$ or $C_2H_5OCN$. Thus, electronic structure calculations of the bond energy and vibrational frequencies of both isomers were made using a commercial program (HyperChem).[49] This program could also be used to calculate the energy and physical properties of the lowest excited triplet states of these molecules. The calculations were made at the 6-311++G$^{**}$/MP2 level of theory; thus, the uncertainty in the calculations is large (± 80 kJ mol$^{-1}$). The vibrational frequencies were calculated using a smaller basis set at the 6-311G$^*$/MP2 level of theory. The results of the electronic structure calculations are summarized in Table 8.

## IV. Discussion

### A. The recombination channel, 1d

Troe's description[2] of a high-pressure recombination rate constant, $k_{rec,\infty}$, was used to provide a theoretical estimate for $k_{1d}$. In this formulation, $k_{rec,\infty}$ is given by:

$$k_{rec,\infty} = \frac{kT}{h}\left(\frac{h^2}{2\pi\mu kT}\right)^{3/2} \frac{Q_{el}(AB)}{Q_{el}(A)\,Q_{el}(B)} \frac{Q^*_{cent} F^*_{AMe} \frac{1}{\sigma^*}}{Q_{vr}(A)\,Q_{vr}(B)} \times \prod^{b} Q^*_j \prod^{r} Q^*_m \exp\left(-\frac{\Delta E_{0z}}{kT}\right) \quad \text{(E1)}$$

where $k$, $h$, and $T$ have their usual meaning, $\mu$ is the reduced mass, $Q_{el}(X)$ is the electronic partition function of X, $Q^*_{cent}$ is a

**Table 6** Summary of the reactions and rate constants used to model the NCO + $n$-$C_4H_{10}$ system at 294 K

| No. | Reactants | | Products | $k$/cm$^3$ molecule$^{-1}$ s$^{-1}$ | Ref. |
|---|---|---|---|---|---|
| 4a | NCO + $n$-$C_4H_{10}$ | → | HNCO + 1-$C_4H_9$[a] | Optimized[a] | |
| 4b | | | HNCO + 2-$C_4H_9$[a] | | |
| 5 | NCO + NCO | → | $N_2$ + 2CO | $(5.0 \pm 2.0) \times 10^{-12}$ | 24 |
| 12a | NCO + $C_4H_9$ | → | HNCO + $C_4H_8$ | $5.0 \times 10^{-11}$ | Guess |
| 12b | | → | $C_4H_9NCO$ | $2.0 \times 10^{-10}$ | |
| 13 | NCO + $C_4H_8$ | → | Products1 | $1.0 \times 10^{-10}$ | Guess |
| 14 | NCO + $C_8H_{18}$ | → | Products2 | $2.0 \times 10^{-10}$ | Guess |
| 15 | NCO + $C_4H_9O_2$ | → | Products3 | (1.0 to 50) × $10^{-12}$ | Varied |
| 16a | Cl + $n$-$C_4H_{10}$ | → | HCl + 1-$C_4H_9$ | $(6.2 \pm 0.7) \times 10^{-11}$ | 44 |
| 16b | | → | HCl + 2-$C_4H_9$ | $(1.5 \pm 0.2) \times 10^{-10}$ | |
| 17a | n-$C_4H_9$ + $n$-$C_4H_9$ | → | $C_8H_{18}$ | $(1.7 \pm 0.2) \times 10^{-11}$[b] | 45, 46 |
| 17b | | → | $C_4H_{10}$ + $C_4H_8$ | $(3.2 \pm 0.4) \times 10^{-12}$[b] | |
| 18 | $C_4H_9$ + $O_2$ | → | $C_4H_9O_2$[c] | $1.4 \times 10^{-11}$[c] | 47 |
| 19 | X | Diff. | X | Measured/calculated | |

[a] The distribution of 1-$C_4H_9$ and 2-$C_4H_9$ radicals as in reaction (16). [b] $k_{17}$ was assumed to be the same for all $C_4H_9$ isomeric combinations. [c] $k_{18}$ was assumed the same for all $C_4H_9$ isomers.

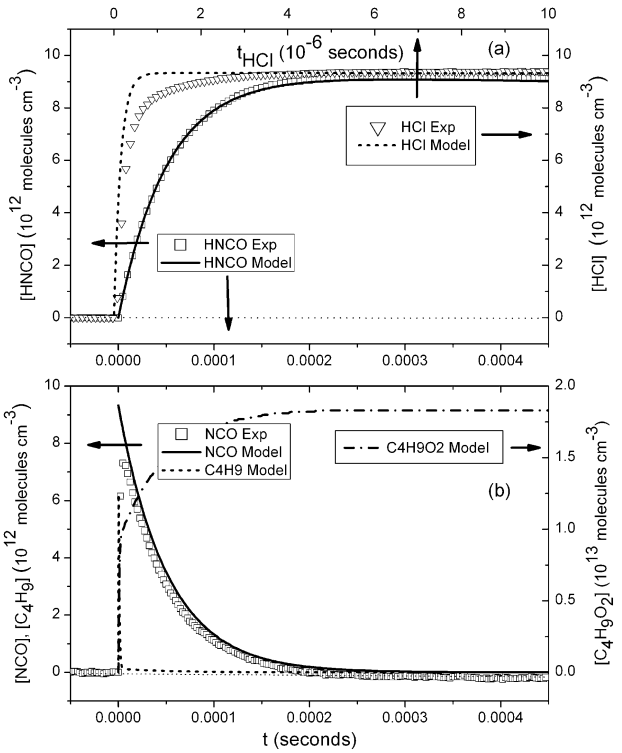


**Fig. 6** (a) Typical concentration temporal profiles for HCl (▽) and HNCO (□) used to determine $\sigma_{pk}^{HNCO}$ for the $\nu_1$ $^qR_0(16)$ transition. The experimental points are shown every 10th point. The curves are the model simulations for HNCO (—) and HCl (–···-). The HNCO profile was fit by varying $k_4$ and $\sigma_{pk}^{HNCO}$ as described in the text. For this experiment $k_4$ was found to be $(5.8 \pm 0.3) \times 10^{-13}$ cm$^3$ molecule$^{-1}$ s$^{-1}$ and $\sigma_{pk}^{HNCO}$ was $(5.12 \pm 0.05) \times 10^{-18}$ cm$^2$ molecule$^{-1}$. For this simulation, $k_{15}$ was $1.0 \times 10^{-12}$ cm$^3$ molecule$^{-1}$ s$^{-1}$. The conditions of the experiment were $P_{O_2} = 2.62$, $P_{n\text{-}C_4H_{10}} = 1.011$, $P_{Ar} = 0.401$, and $P_{ClNCO} = 0.014$ Torr at 294 K. (b) Same as (a) except the experimental profile for NCO (□) is shown. The model NCO (—) profile using $k_4$ determined in (a). The value of $k_4$ that was found by fitting the NCO profile was $(6.7 \pm 0.4) \times 10^{-13}$ cm$^3$ molecule$^{-1}$ s$^{-1}$, and the initial value of $\sigma_{pk}^{HNCO}$ was $(5.09 \pm 0.1) \times 10^{-18}$ cm$^2$ molecule.$^{-1}$ The model $C_4H_9$ (···) profile and indicates how effective reaction (15) is at scavenging the butyl radicals. The model profile for $C_4H_9O_2$ (- ··· -).

centrifugal pseudo-partition function, $F^*_{AME}$ is a factor correcting for the rotation character of the disappearing oscillators, $\sigma^*$ is the effective symmetry number at the transition state, $Q_{vr}(X)$ is the rovibrational partition function of X, $Q_j^*$ is the vibrational partition function for the conserved modes of AB, $Q_m^*$ is the vibrational partition function for the transitional modes, and $\Delta E_{0z}$ is the lowest threshold energy for recombination. The new bond is described by Morse potential energy parameters and an interpolation parameter, $\alpha$, describing the transformation of rotational degrees of freedom in the radical fragments into transitional modes of the new molecule.

In a systematic study, Cobos and Troe[50] found that values of $\alpha/\beta$ equal to $0.46 \pm 0.09$ provided agreement between calculated and experimental values of $k_{rec,\infty}$ for over 26 systems. The theoretical estimates of $k_{rec,\infty}$ for reaction (1d) are reported in Table 9 for $\alpha/\beta$ equal to the average and the plus and minus limits found by Cobos and Troe. Even though the experimental rate constants are in the fall-off region at a pressure of 4.5 Torr, the values of $k_{1d}$ (Fig. 5a) are about a factor of five larger than the theoretical estimates for $\alpha/\beta = 0.55$ (Table 9). An increase in either the bond dissociation energy by a 100 kJ mol$^{-1}$ or the $\alpha/\beta$ ratio to 1.1 only increases the calculated value of $k_{rec,\infty}$ by a factor of two, and is still more than a factor of two smaller than the experimental value.

The value of $k_{rec,\infty}$ could be increased if the electronic degeneracy factor in eqn (E1) was larger than the statistical value of 1/8. This would require the participation of the triplet spin manifold in the reaction dynamics. There are several ways this could occur. By direct recombination into the triplet manifold followed by intersystem crossing (ISC) to the ground state, as suggested by Smith[51] or indirectly by increasing the effective density of states due to the mixing of the singlet and triplet manifolds by the spin–orbit interaction in NCO. This mechanism was proposed by Sims and Smith[52] to account for the larger than expected recombination rate constant for CN and NO radicals. However, neither of these mechanisms is likely to be operative in the NCO + $C_2H_5$ system. The initial approach of the two radicals on the $C_2H_5NCO/OCN$ ($a^3A''$)

**Table 7** Summary of the experimental conditions and results for the determination of $\sigma_{pk}^{HNCO}$ and $k_4$ using the model chemistry[a] in Table 6

| Partial pressure | | | $k_4$/cm$^3$ molecules$^{-1}$ s$^{-1}$ | | |
|---|---|---|---|---|---|
| $P_{O_2}$ | $P_{n\text{-}C_4H_{10}}$ | NCO ($10^{12}$)[b] | NCO profile ($10^{-13}$) | HNCO profile ($10^{-13}$) | $\sigma_{pk}^{HNCO}$ ($10^{-18}$)[c] |
| 2.301 | 1.93 | 4.51 | 4.8 | 4.7 | 5.9 |
| | | 7.24 | 5.7 | 5.1 | 4.7 |
| 2.70 | 1.45 | 3.08 | 4.7 | 5.0 | 5.7 |
| | | 5.51 | 5.3 | 4.8 | 5.7 |
| 1.65 | 0.487 | 9.13 | 6.5 | 6.1 | 4.7 |
| | | 2.92 | 5.2 | 5.5 | 5.7 |
| 1.76 | 0.370 | 3.33 | 5.3 | 5.2 | 5.6 |
| 1.90 | 0.267 | 3.86 | 6.8 | 4.9 | 4.3 |
| 3.00 | 0.654 | 5.10 | 4.9 | 4.9 | 4.8 |
| | | 8.84 | 5.9 | 5.3 | 5.0 |
| 2.62 | 1.01 | 18.0 | 7.3 | 6.0 | 4.7 |
| | | 9.33 | 6.7 | 5.8 | 5.1 |
| | | 4.71 | 5.4 | 5.0 | 5.7 |
| Average | | | 5.7 | 5.3 | 5.2 |
| Standard deviation | | | ±0.86 | ±0.51 | ±0.53 |

[a] The reported determinations were obtained with $k_{15}$ equal to $1.0 \times 10^{-12}$ cm$^3$ molecule$^{-1}$ s$^{-1}$. [b] Units, molecules cm$^{-3}$. [c] Units, cm$^2$ molecule$^{-1}$.

 

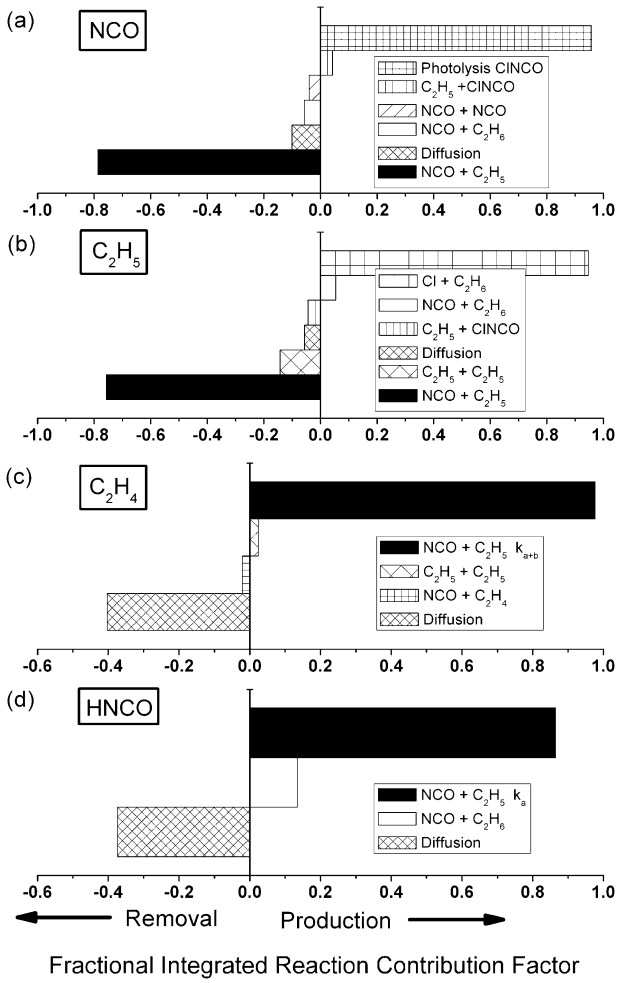


**Fig. 7** An IRCF analysis plotted as a fraction of the total removal (negative) and total production (positive) fluxes for each major species in reaction (1) under conditions of low total pressure and low $P_{C_2H_6}$ corresponding to the experiment in Fig. 1. (a) NCO. (b) $C_2H_5$. (c) $C_2H_4$. (d) HNCO.

PES is likely repulsive because of the similar orbital and spin alignments; thus, direct recombination on this PES is unlikely. The theoretical calculations reported in section IV F placed the energy of the triplet state for either isomer higher in energy than the energy asymptote of the products. At best, the triplet state density will be low in this region and not enhance the density of states. No information about the $C_2H_5NCO/OCN$ ($b^3A'$) PES is available except to note that the bonding interaction will be even smaller because the two radical orbitals are orthogonal. High-level electronic structure calculations on the excited states of the related H + NCO system concur with these simple arguments.[53]

**Table 8** Theoretical estimates of the bond energies and morse parameters for the dissociating bonds $C_2H_5$–NCO and $C_2H_5$–OCN producing NCO + $C_2H_5$

| Isomer | Dissociation energy (D)[a] ($X^1A'$)/kJ mol$^{-1}$ | $\beta^b$/Å$^{-1}$ | $\nu_D$/cm$^{-1}$ |
|---|---|---|---|
| $C_2H_5$–NCO | 240 | 2.63 | 778 |
| $C_2H_5$–OCN | 250 | 3.91 | 1176 |

[a] Calculated at the 6-311++G*/MP2 level of theory and corrected for zero point energy. [b] Morse parameter, $\beta = \sqrt{2\pi^2\mu/Dh^2}$.

**Table 9** Estimates for $k_{rec,\infty}$ for the NCO + $C_2H_5$ reaction producing $C_2H_5NCO$ or $C_2H_5OCN$ ($X^1A'$) at 300 K

| | $k_{rec,\infty}$/cm$^3$ molecule$^{-1}$ s$^{-1}$ | | |
|---|---|---|---|
| Product | $\alpha/\beta = 0.46$ | $\alpha/\beta = 0.55$ | $\alpha/\beta = 0.37$ |
| $C_2H_5NCO$ | $1.9 \times 10^{-11}$ | $3.8 \times 10^{-11}$ | $7.7 \times 10^{-12}$ |
| $C_2H_5OCN$ | $1.4 \times 10^{-11}$ | $3.3 \times 10^{-11}$ | $4.2 \times 10^{-12}$ |

It has been recognized that the long-range portion of the PES between two radicals can play an important part in the reaction dynamics.[54] In this region, the various forms of angular momentum start to couple to the collision frame. For atoms with electronic angular momentum reacting with molecules or radicals, theoretical calculations by several groups have shown that non-adiabatic transitions can occur in the van der Waals region of the PES if the spin–orbit splitting of the atom is smaller than the van der Waals well depth. Schatz and coworkers[55,56] illustrated this for Cl($^2$P) + HCl reaction by artificially adjusting the spin–orbit constant in the chlorine atom. Similarly, Takayanagi *et al.*[57] conducted high level, MRCI cc-pVDZ and cc-pVTZ, theoretical calculations on the 5 doublet PESs for the N($^2$D) + $C_2H_2$ reaction, and calculated the rate constant as a function of temperature. They concluded that non-adiabatic effects induced at large internuclear separations increased the effective electronic degeneracy for the reaction. The relationship between spin–orbit splitting and van der Waals well depth is further illustrated by the theoretical calculations by Yagi *et al.*[58] on the O($^3$P) + $CH_3$(X $^2A_2''$) reaction. They showed that non-adiabatic transitions did not play a direct role in the reaction dynamics. For this system, the fine-structure splittings in the O atom are comparable to the van der Waals well depth.

The enhancement of the electronic degeneracy factor by the long range mixing of electronic states could be important in radical–radical reactions involving the NCO radical. For this mechanism to be operative the important parameter appears to be the ratio of the spin–orbit constant to the van der Waals well depth. For linear NCO(X $^2\Pi$), the fine-structure splitting is 95.6 cm$^{-1}$; however, NCO is subject to the Renner–Teller effect and the electronic angular momentum is quenched as the molecule bends. Thus, the effective spin–orbit constant in the NCO + $C_2H_5$ system could be smaller in bent configurations involving the NCO molecular frame enhancing non-adiabatic effects. Theoretical calculations on the quenching of NCO electronic angular momentum in the presence of species possessing unpaired electrons will need to be done to determine if this mechanism is possible.

### B. Abstraction or complex formation, channels (1a) and (1b)

As is evident from Fig. 5b, $k_{1a}$ and $k_{1b}$ are independent of pressure within the scatter in the data, and suggests that these two product channels could be produced in a direct bimolecular collision encounter. The radical orbital on NCO has predominantly N atom p-orbital character so that the

dominant abstraction product would be expected to be the HNCO + $C_2H_4$ product channel as observed.

If channel (1a) is indeed an abstraction process, the interaction of NCO with $C_2H_5$ must be substantially different from the interaction with $C_2H_6$, especially on a per H atom basis. The temperature dependence[22] of $k_2$ has been measured. If it is represented by a simple Arrhenius expression, the Arrhenius factor is $1.0 \times 10^{-11}$ and the activation energy is 15.9 kJ $mol^{-1}$. This activation energy is in excellent agreement with a theoretical calculation for the barrier height.[59] At room temperature, on a per hydrogen atom basis, the NCO abstraction rate of a hydrogen atom from $C_2H_5$ compared to $C_2H_6$ is $1.3 \times 10^4$ times larger; however, a reduction of the barrier height to zero can only account for a factor of $5.9 \times 10^2$ in the reactivity. The remaining enhancement of the abstraction efficiency by a factor of 20 could be due to a larger acceptance angle for the NCO + $C_2H_5$ reaction or the dynamical role played by the energy released in the formation of the more stable $C_2H_4$ molecule rather that the $C_2H_5$ radical. This is in contrast to the usual view of abstraction reaction dynamics being governed by repulsive energy release between the breaking bond fragments such as occurs the related $Cl(^2P)$ + $C_2H_6$.[60]

The formation of channels (1a) and (1b) could also result through complex formation if isomerization and bond breaking occur before collisional stabilization. The formation of a complex would be dominated by the initial overlap of the half-occupied p-orbitals on the carbon and nitrogen atoms; however, this interaction would lead to a $\beta$-H atom transfer and the preferential formation of HOCN + $C_2H_4$ products rather than the observed HNCO + $C_2H_4$ ones. For the isoelectronic reaction, $O_2$ + $C_2H_5$ → $C_2H_4$ + $HO_2$, theoretical calculations[61] have revealed that the dominant low temperature pathway is a concerted-elimination route through a five-membered ring intermediate formed from the initial $C_2H_5O_2$ adduct. A similar reaction path from a $H_3CH_2\cdots$NCO intermediate by a six-membered ring intermediate would produce HOCN + $C_2H_4$ products. If the initial interaction involved a $H_3CH_2\cdots$OCN adduct, this concerted-elimination pathway would lead to HNCO + $C_2H_4$ products. From an $H_3CH_2\cdots$NCO adduct, the abstraction of an α-hydrogen atom to form HNCO followed by a hydrogen atom transfer from the methyl group to form $C_2H_4$ would have a significant energy barrier. This pathway is similar to the formation of the OH + $CH_3CHO$ channel in the $O_2$ + $C_2H_5$ reaction by α-hydrogen atom migration and decomposition from the initial $C_2H_5O_2$ adduct. Calculations[61] show that this pathway has a larger barrier than the concerted-elimination pathway.

### C. Channel (1c)

The only observed product from channel (1c) was HCN. The coproduct was assumed to be the most stable one, $CH_3CHO$. The HNC isomer of HCN, was not observed. Clearly, the formation of HCN + $CH_3CHO$ in reaction (1) requires isomerization and bond breaking from a $C_2H_5\cdots$NCO/OCN intermediate. A plausible pathway is α-hydrogen migration to the carbon atom of OC′N by the formation of a four-membered ring transition state followed by C′–O bond cleavage giving HCN and $H_3CHO$ products. This pathway is again similar to the α-hydrogen migration in the $C_2H_5O_2$ adduct alluded to in the previous paragraph. A four-centered transition state involving NCCC atoms has been discovered to be the lowest energy pathway in the NCO + $C_2H_2$ reaction.[62]

### D. Estimated uncertainties in $k_1$, $k_{1a}$ and $k_{1a}$ + $k_{1b}$

The uncertainties in the rate constants are directly related to the factors that determine the concentrations of the various species monitored in the experiment, either directly by a concentration measurement or indirectly through the uncertainties in the rate constants used to the model analysis. The uncertainty in the concentration measurement of each observed species is given by the sum of the uncertainties in the absorption coefficient (Table 1) and the path length, which is small, ± 0.2% (section II). The uncertainties in the concentration measurements introduced by the uncertainties in the rate constants used in the model calculations were estimated using the results of the $IRCF^X$ analysis for each experiment (Fig. 7), as described in several recent works.[16,63,] To a good approximation, the propagation error in a specific rate constant is given by the fraction of the total removal flux for that specific reaction times the rate constant uncertainty.

The IRCF analysis in Fig. 7 is typical of the experimental conditions used to measure $k_1$. There were only four reactions contributing to NCO kinetics beside reaction (1), reactions (2), 5, (10) and $k_{diff}^{NCO}$. The uncertainty in $k_2$ was taken to be ±15% based on the difference between the value used to analyze the data (Table 2) and the value measured in this work (Table 5). At low pressures of $C_2H_6$, reaction (2) contributed about 10% to the total removal of NCO; thus, the uncertainty in $k_2$ contributed about ±1.5% to the systematic uncertainty in the determination of $k_1$. Reactions (5) and (10) are production processes but contributed less than 5% to the total NCO production flux, and hence, contributed about ±3% each to the uncertainty in $k_1$. Assuming the uncertainties in the parameters used to define the NCO concentration were distributed randomly, they contributed a total systematic uncertainty of ±7% to the determination of $k_1$.

The concentration of $C_2H_5$ was not directly monitored in the experiment, but was established by the initial radical concentration and the kinetic model. The initial NCO and $C_2H_5$ radical concentrations were determined from the HCl profile, contributing a systematic uncertainty of ±1% due to the uncertainty in $\sigma_{pk}^{HCl}$ (Table 1). The reactions contributing directly to the $C_2H_5$ concentration besides reaction (1) were reactions (2), (9), (10), and $k_{diff}^{C_2H_5}$. The uncertainties in the individual reactions are listed in Table 2 and can be combined with the IRCF $^{C_2H_5}$ from Fig. 7 to provide an overall estimate of the uncertainty in the $C_2H_5$ concentration, and hence contributing an uncertainty of ±7% to $k_1$, coincidentally the same as for NCO.

Other factors effecting the measurements such as pressure broadening, flow and total pressure measurements, and the uncertainty in tuning to the maximum of an absorption feature were small or contribute to the random scatter in the measurements of $k_1$. This random scatter was taken from Table 4 to be ±13%. Assuming the individual errors were distributed randomly, the systematic and random errors were

 

combined to give an estimated uncertainty in $k_1$ of ±16%, including both systematic and random errors.

A similar analysis as outlined above can be used to estimate the contribution of systematic and random errors in the measurements of $k_{1a}$ and $k_{1b}$. Both HNCO and $C_2H_4$ were removed by diffusion with an experimental uncertainty of ± 10% (section III. B). Reaction (2) produced HNCO with an uncertainty in $k_2$ of ±15%, as discussed. There were no significant reactions producing $C_2H_4$ (Fig. 7c). The largest uncertainty in analyzing the HNCO profile resulted from the uncertainty of ±11% in the value of $\sigma_{pk}^{HNCO}$ (Table 1). The $\sigma_{pk}{}^{C_2H_4}$ is better known and has an uncertainty of ±1% (Table 1). The uncertainties in the determination of the HNCO and $C_2H_4$ concentrations were calculated to be ±12 and ±4%, respectively. However, the determination of $k_{1a}$ and $k_{1a} + k_{1b}$ relied on the NCO and $C_2H_5$ concentrations as well, contributing uncertainties of ±7% each. Again, combing these uncertainties with a random scatter of ±16% in $k_{1a}$ and $k_{1a} + k_{1b}$ (Table 4), the resultant random and systematic errors in $k_{1a}$ and $k_{1a} + k_{1b}$, were ±22% from the HNCO profile analysis for $k_{1a}$ and ±19%, if the $C_2H_4$ profile had been analyzed to determine both $k_{1a} + k_{1b}$.

It is worth mentioning again that the contributions to the secondary chemistry change significantly at higher $C_2H_6$ partial pressure. However, the rate constants for reaction (1) derived under the high $C_2H_6$ partial pressure conditions (Table 5) were similar to those found under low partial pressure conditions, indicating that the rate constants used in the model analysis were close to their true values.

## V. Summary

The rate constant for the NCO + $C_2H_5$ reaction was measured over a pressure range of 2.1 to 4.4 Torr at a temperature of 293 ± 2 K, and found to increase with increasing pressure. Over this pressure range $k_1$ is represented by $(1.25 \pm 0.16) \times 10^{-10} + (3.3 \pm 0.47) \times 10^{-11}$ $P$(Torr) cm$^3$ molecules$^{-1}$ s$^{-1}$ (Fig. 5a), where the uncertainties are the standard deviation in the fit parameters. The combined systematic and random error in the measurements in $k_1$, was estimated to be ±16% at the 1$\sigma$ level.

The rate constants for the three pressure independent channels (Fig. 5b and c) were measured to be: 1a (HNCO + $C_2H_4$), $k_{1a} = (1.1 \pm 0.16) \times 10^{-10}$ cm$^3$ molecule$^{-1}$ s$^{-1}$, 1b (HOCN + $C_2H_4$), $k_{1b} = (2.9 \pm 1.3) \times 10^{-11}$ cm$^3$ molecule$^{-1}$ s$^{-1}$, and 1c (HCN + $H_3CCHO$) $k_{1c} = (8.7 \pm 1.5) \times 10^{-13}$ cm$^3$ molecule$^{-1}$ s$^{-1}$, where the uncertainty is 1$\sigma$ in the scatter of the data. Channel 1d was pressure dependent with $k_{1d} = (0.090 \pm 1.3) \times 10^{-11} + (5.21 \pm 0.36) \times 10^{-11}$ $P$(Torr) cm$^3$ molecule$^{-1}$ s$^{-1}$ (Fig. 5a).

The data analysis also resulted in the measurement of other rate constants: $k_2 = (1.6 \pm 1.1) \times 10^{-14}$ cm$^3$ molecule$^{-1}$ s$^{-1}$, $k_4 = (5.3 \pm 0.51) \times 10^{-13}$ cm$^3$ molecule$^{-1}$ s$^{-1}$, and $k_{10} = (2.3 \pm 1.2) \times 10^{-13}$ cm$^3$ molecule$^{-1}$ s$^{-1}$, where the uncertainty is 1$\sigma$.

The pressure independence of channels (1a) and (1b) and the dominance of channel (1a) suggest that these two channels proceed by in a direct bimolecular collision and are the result of an abstraction process rather than complex formation.

The participation of electronically excited states in the reaction dynamics was examined. A possible mechanism causing the large rate constant for reaction (1) could be the mixing of triplet and singlet manifolds at long range due to the spin–orbit interaction in NCO, thus leading to an enhanced electronic degeneracy factor for the reaction.

## Acknowledgements

This work was performed under the auspices of the Office of Basic Energy Sciences, Division of Chemical Sciences, Geosciences, and Biosciences, US Department of Energy, under contract number DE-AC02-06CH11357.

## References

1 W. C. Gardiner, Jr, *Gas-Phase Combustion Chemistry*, Springer-Verlag, New York, 1999.
2 J. Troe, *J. Chem. Phys.*, 1981, **75**, 226.
3 I. W. M. Smith, *J. Chem. Soc., Faraday Trans.*, 1991, **87**, 2271.
4 V. D Knyazev and I. R. Slagle, *J. Phys. Chem. A*, 2001, **105**, 6490.
5 E. V Shafir, I. R. Slagle and V. D. Knyazev, *J. Phys. Chem. A*, 2003, **107**, 6804.
6 S. I. Stoliarov, V. D. Knyazev and I. R. Slagle, *J. Phys. Chem. A*, 2000, **104**, 9687.
7 D. G. Truhlar, B. C. Garrett and S. J. Klippenstein, *J. Phys. Chem.*, 1996, **100**, 12771.
8 S. J. Klippenstein, Y. Georgievkii and L. B. Harding, *Phys. Chem. Chem. Phys.*, 2006, **8**, 1133.
9 L. B. Harding, S. J. Klippenstein and Y. Georgievski, *Proc. Combust. Inst.*, 2005, **30**, 985.
10 J. A. Miller and C. T. Bowman, *Prog. Energy Combust. Sci.*, 1989, **15**, 277.
11 C. P. Fenimore, *Thirteenth Symposium (International) on Combustion*, The Combustion Institute, Pittsburgh, 1971, p. 373.
12 K. J. Huges, A. S. Tomlin, E. Hampartsoumian, W. Nimmo, I. G. Zsély, M. Ujvári, T. Turănyi, A. R. Clague and M. J. Pilling, *Combust. Flame*, 2001, **124**, 573.
13 B. A. Williams and J. W. Fleming, *Comb. Flame*, 1997, **110**, 1.
14 Y. Gao and R. G. Macdonald, *J. Phys. Chem. A*, 2006, **110**, 977.
15 G. He, I. Tokue, L. B. Harding and R. G. Macdonald, *J. Phys. Chem. A*, 1998, **102**, 7653.
16 Y. Gao and R. G. Macdonald, *J. Phys. Chem. A*, 2005, **109**, 5388.
17 A. S. Pine, A. Fried and J. W. Elkins, *J. Mol. Spectrosc.*, 1985, **109**, 30.
18 M. Dang-Nhu, A. S. Pine, A. Fayt, M. de-Veleeschouwer and C. Lambeau, *Can. J. Phys.*, 1983, **61**, 514.
19 HITRAN 2004 edition, http://cfa-www.harvard.edu/hitran/; L. S. Rothman, D. Jacquemart, A. Barbe, D. C. Benner, M. Birk, L. R. Brown, M. R. Carleer, C. Chackerian, Jr, K. Chance, L. H. Coudert, V. Dana, V. M. Devi, J.-M. Flaud, R. R. Gamache, A. Goldman, J.-M. Hartmann, K. W. Jucks, A. G. Maki, J.-Y. Mandin, S. T. Massie, J. Orphal, A. Perrin, C. P. Rinsland, M. A. H. Smith, J. Tennyson, R. N. Tolchenov, R. A. Toth, J. V. Auwera, P. Varanasi and G. Wagner, *J. Quantum Spectrosc. Radiat. Transfer*, 2004, **96**, 139.
20 K. M. T. Yamada, M. Winnewisser and J. W. C. Johns, *J. Mol. Spectrosc.*, 1990, **140**, 353.
21 H. W. Kroto, *Molecular Rotational Spectra*, Dover, New York, 1992.
22 K. H. Becker, H. Geiger, F. Schmidt and P. Wiesen, *Phys. Chem. Chem. Phys.*, 1999, **1**, 5305.
23 J. Park and J. F. Hershberger, *Chem. Phys. Lett.*, 1994, **218**, 537.
24 S. Wategaonkar and D. W. Setser, *J. Phys. Chem.*, 1993, **97**, 10028.
25 J. S. Pilgrim, A. McIlroy and C. A. Taatjes, *J. Phys. Chem. A*, 1997, **101**, 1873.
26 W. E. Falconer and W. A. Sunder, *Int. J. Chem. Kinet.*, 1971, **3**, 523.
27 M. A. A. Clyne and A. J. MacRobert, *J. Chem. Soc., Faraday Trans. 2*, 1983, **79**, 283.

28 M. S. Schuurman, S. R. Muir, W. D. Allen and H. F. Schaefer III, *J. Chem. Phys.*, 2004, **120**, 11586.
29 B. Ruscic, J. E. Boggs, A. Burcat, A. G. Császár, J. Demaison, R. Janoschek, J. M. L. Martin, M. L. Morton, M. J. Rossi, J. F. Stanton, P. G. Szalay, P. R. Westmoreland, F. Zabel and T. Bérces, *J. Chem. Ref. Data*, 2005, **34**, 573.
30 A. Bodi, J. P. Kercher, C. Bond, P. Meteesatien, B. Sztaray and T. Baer, *J. Chem. Phys. A*, 2006, **110**, 13425.
31 S. S. Xantheas, T. H. Dunning, Jr and A. Mavridis, *J. Chem. Phys.*, 1997, **106**, 3280.
32 L. V. Gurvich, I. V. Veyts and C. B. Alcock, *Thermodynamic Properties of Individual Substances*, 4th edn, Hemisphere Pub. Co., New York, 1989.
33 J. C. Rienstra-Kiracofe, W. D. Allen and H. F. Schaeffer III, *J. Phys. Chem. A*, 2000, **104**, 9823.
34 A. Burcat, http://ftp.technion.ac.il/pub/supported/aetdd/thermodynamics/2003.
35 A. Schuck, H. Volpp and J. Wolfrum, *Combust. Flame*, 1994, **99**, 491.
36 C. J. Astbury, G. Hancock and K. G. McKendrick, *J. Chem. Soc., Faraday Trans.*, 1993, **89**, 405.
37 J. A. Fernández, P. Puyuelo, D. Husain, M. N. S. Rayo and F. Castaño, *J. Chem. Phys.*, 1997, **106**, 7090.
38 E. N. Fuller, K. Ensley and C. J. Giddings, *J. Phys. Chem.*, 1969, **73**, 3679.
39 P. W. Seakins, E. L. Woodbridge and S. R. Leone, *J. Phys. Chem.*, 1993, **97**, 5633.
40 M. M. Maricq, J. J. Szente and E. W. Kaiser, *J. Phys. Chem.*, 1993, **97**, 7970.
41 J. T. Yardley, *Introduction to Molecular Energy Transfer*, Academic Press, New York, 1980.
42 R. C. L. Yaun and G. W. Flynn, *J. Chem. Phys.*, 1972, **57**, 1316.
43 R. C. L. Yaun, J. M. Preses, G. W. Flynn and A. M. Ronn, *J. Chem. Phys.*, 1973, **59**, 6128.
44 G. S. Tyndall, J. J. Orlando, T. J. Wallington, M. Dill and E. W. Kaiser, *Int. J. Chem. Kinet.*, 1996, **29**, 43.
45 V. D. Knyazev and I. R. Slagle, *J. Phys. Chem.*, 1996, **100**, 5318.
46 W. E. Morganroth and J. G. Calvert, *J. Am. Chem. Soc.*, 1966, **88**, 5387.
47 T. M. Lenhardt, C. E. McDade and K. D. Bayes, *J. Chem. Phys.*, 1980, **72**, 304.
48 J. Warnatz, U. Maas and R. W. Dibble, *Combustion: Physical and Chemical Fundamentals, Modeling and Simulation, Experiments Pollutant Formation*, Springer, Berlin, 1995.
49 HyperChem. Hypercube, Inc.: Gainsville, FL, 32601.
50 C. J. Cobos and J. Troe, *J. Chem. Phys.*, 1985, **83**, 1010.
51 I. W. M. Smith, *Int. J. Chem. Kinet.*, 1984, **16**, 423.
52 I. R. Sims and I. W. M. Smith, *J. Chem. Soc., Faraday Trans.*, 1993, **89**, 1.
53 E. F. Valeev, W. D. Allen, H. F. Schaefer III, A. G. Császár and A. L. L. East, *J. Chem. Phys.*, 2001, **105**, 2716.
54 M. M. Graff and A. F. Wagner, *J. Chem. Phys.*, 1990, **92**, 2423.
55 G. C. Schatz, *J. Phys. Chem.*, 1995, **99**, 7522.
56 G. C. Schatz, P. McCabe and J. N. L. Connor, *Faraday Discuss.*, 1998, **110**, 139.
57 T. Takayanagi, Y. Kurosaki, K. Yokoyama, K. Sato and S. Tsunashima, *Chem. Phys. Lett.*, 1999, **312**, 503.
58 K. Yagi, T. Takayanagi, T. Taketsugu and K. Hirao, *J. Chem. Phys.*, 2004, **120**, 10395.
59 H. T. Chen and J. J. Ho, *J. Phys. Chem.*, 2003, **107**, 7643.
60 M. J. Bass, M. Brouard, C. Vallance, T. N. Kitsopoulos, P. C. Samartzis and R. L. Toomes, *J. Chem. Phys.*, 2003, **119**, 7168.
61 J. C. Rienstra-Kiracofe, W. D. Allen and H. F. Schaefer III, *J. Phys. Chem. A*, 2000, **104**, 9823.
62 H. Xie, J. Wang, S. Zhang, Y. Ding and C. Sun, *J. Chem. Phys.*, 2006, **125**, 124317.
63 M. Bahng and R. G. Macdonald, *J. Phys. Chem. A*, 2007, **111**, DOI: 10.1021/jpo66359c.